JOURNAL OF MATERIALS PROCESSING TECHNOLOGY 199 (2008) 41–48

journal homepage: www.elsevier.com/locate/jmatprotec

Finite element modeling of electron beam welding of a large complex Al alloy structure by parallel computations

Yanhong Tian[a,*], *Chunqing Wang*[a], *Danyang Zhu*[b], *Y. Zhou*[c]

[a] *State Key Laboratory of Advanced Welding Production Technology, Harbin Institute of Technology, Harbin 150001, China*
[b] *School of Materials Science and Engineering, Harbin Institute of Technology, Harbin 150001, China*
[c] *Centre for Advanced Materials Joining, Department of Mechanical Engineering, University of Waterloo, Waterloo, Ontario, Canada N2L 3G1*

ARTICLE INFO

Article history:
Received 2 December 2005
Received in revised form
4 April 2006
Accepted 25 July 2007

Keywords:
Electron beam welding
Parallel calculation
Keyhole
Pre-deformation
Al alloy structure

ABSTRACT

This paper describes features of a three-dimensional finite element model to simulate the temperature field of a large complicated Al alloy structure during electron beam welding (EBW), aiming to control the final distortion of the welded structure. The actual workpiece is about 1 m in length, with over 8 m aggregate weld length. Because a much finer mesh was required to describe the electron beam heat source, computational work would be substantially increased due to the three-dimensional model. In order to improve calculation speed and quality of simulation, parallel calculation was performed by establishing a computer cluster system composed of four PCs. At the same time, a dynamic three-dimensional keyhole was applied in this model to simulate the heat generation in the cavity. Following the heat source, the keyhole moved along the weld line, allowing a more complex expression to describe the heat source of EBW. Several welding process parameters including input energy and welding speed were studied systematically, as well as the influence of pre-deformation before welding on the ultimate distortion. The results show that the input energy and welding speed have a direct effect on the temperature field, especially on the shape and dimensions of the weld pool, and they seriously influence the final distortion. Pre-deformation also has an effect on distortion, but not apparently as strong as the parameters mentioned above.

1. Introduction

Electron beam welding (EBW) has unique advantages over other traditional fusion welding methods due to high-energy density, deep penetration, large depth-to-width ratio and small heat affected zone (HAZ). During the EBW process, the molten metal in the weld joint is heated and locally vaporized by the high-energy density of the electron beam, resulting in a keyhole (Tong and Gied, 1970). Unlike many other fusion welding methods which only heat the surface of the weld joint, the EBW heat source can put the energy through the thickness of the workpiece via the keyhole. Thus, it is necessary to take the keyhole shape into consideration when an EBW thermal source model is established. Many analytical 2-D or 3-D models of the electron beam thermal source have been developed in the literature. Couedel et al. (2003) established a 2-D analytical heat transfer model using a moving thermal source, considering the impact of the source size and the influence of the boundary on the thermal field. Nguyen et al. (1999) introduced an analytical solution for a double-ellipsoidal power

* *Corresponding author*. Fax: +86 451 86416186.
E-mail address: tianyh@hit.edu.cn (Y. Tian).
0924-0136/$ – see front matter © 2007 Elsevier B.V. All rights reserved.
doi:10.1016/j.jmatprotec.2007.07.045

density moving heat source in a semi-infinite body. Wei and Shian (1993) proposed an approximate three-dimensional heat-conduction model by satisfying interfacial energy and momentum balances at the keyhole cavity. He and DebRoy (2003) established a transient, three-dimensional numerical heat transfer and fluid flow model based on the solution of the equations of conservation of mass, momentum and energy to calculate the temperature and velocity fields in the weld pool. Some other authors (Miyazaki and Giedt, 1982; Baeva et al., 1997; Ho and Wei, 1997) also reported various shapes of thermal source, including elliptical cylinder and conical cavity.

Some literature reports related to finite element simulation of welding of large structures have been based on line- or surface-thermal source models (Brown and Song, 1992a,b). The line- and surface-source model could not take the distribution of incident flux into account, and also the vertical heat transport was neglected in the line source model. In the present work, a three-dimensional finite element model for a large structure has been developed in which a keyhole was pre-defined and moved along the weld line, thus Gaussian distribution of thermal source into this dynamic keyhole was considered.

Some finite element algorithms to improve calculation efficiency such as automatic remeshing, adaptive mesh technique and parallel computations have been applied to welding process simulation (Lindgren et al., 1997; Qingyu et al., 2002; Lundbäck, 2003; Lindgren, 2001). In this paper, a parallel calculation algorithm was performed for modeling of temperature field and distortion of a large complex welded structure during electron beam welding. Parallel calculation is an effective means to improve computing speed in finite element analysis. Recently, most parallel calculations were performed by high-performance minicomputer workstations. However, with the rapid development of computer technology, parallel calculation implementation on high-performance personal computers (PCs) has attracted more attention and is now feasible.

The objectives of the present study were: (1) to establish a computer cluster system linked in parallel to perform the modeling and computation job; (2) to establish a new electron beam welding thermal source model, in which heat generation in the cavity was considered by pre-assuming the keyhole dimension; (3) to tackle the distortion problem in local welds coupled with large and complicated structure during electron beam welding based on results of (1) and (2).

2. Finite element modeling

2.1. Parallel calculation

This simulation concerns thermo-mechanical coupled analysis of a large complex welded structure, which imposes high demands on calculation capability and speed of computer. First, the diameter of electron beam interaction zone is so small, in order to describe its behavior exactly, the mesh at the weld position should be several times finer than with other traditional welding methods. Second, the entire welded structure was simulated in this research, comprising 1 m in length with 8 m of weld length in it, which also increases the size of the finite element model. In order to solve the problems of calculation capability and low efficiency of single PC's, parallel calculation technology was implemented by using an ethernet cable connection directly between four computers.

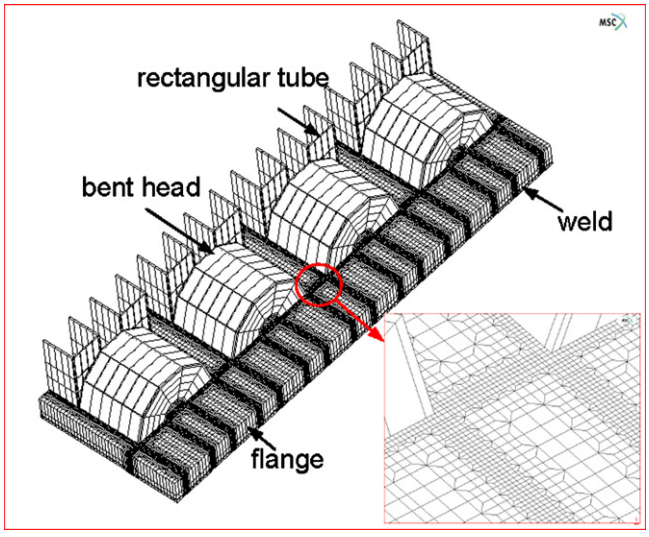

Fig. 1 – Three-dimensional finite element model with bent head, rectangular tube and flange.

2.2. Finite element model

In this simulation, a three-dimensional finite element model for thermo-mechanical coupled analysis was developed using MARC, and a 1/4 finite element model was established based on symmetry characteristics of the Al alloy structure. The model size can best be described by the number of nodes, elements and degrees of freedom. The whole model consisted of 101,984 eight-node hexahedron elements with the capabilities of large deformation and strain. The total number of nodes was 815,872. For temperature field calculation, there were 815,872 degrees of freedom, and for stress and displacement field calculation, there were 2,447,616 degrees of freedom.

These elements were allocated among the four computers of the parallel system, and the total number of time steps was 1600. Fig. 1 shows the finite element model of the Al alloy welded structure including bent head, rectangular tube and flange: both the bent head and the rectangular tube were welded to the flange by electron beam welding. At the welding position, meshes were refined to improve simulation accuracy.

In this study, a keyhole was assumed to be ellipsoidal in shape in any transverse cross-section, with the dimensions of 4 mm depth and 1.57 mm diameter. In the model, the pre-defined cavity moves along the weld line, following the moving heat source. Fig. 2 shows the mesh when a keyhole was formed during the welding process. The keyhole surface was moved and remeshed during the electron beam welding. The shape of the pre-defined keyhole and the movement of the keyhole were controlled by subroutines of MARC software written in Digital Visual Fortran.

Fig. 2 – Mesh and dimensions for pre-assumed keyhole.

2.3. *Heat transfer governing equations*

The heat transfer governing equation for the large complex Al alloy structure in a moving coordinate system with a positive x-direction moving electron beam can be written as

$$\rho C_p \frac{\partial T}{\partial t} = \frac{\partial}{\partial x}\left(k\frac{\partial T}{\partial x}\right) + \frac{\partial}{\partial y}\left(k\frac{\partial T}{\partial y}\right) + \frac{\partial}{\partial z}\left(k\frac{\partial T}{\partial z}\right) - \rho\frac{\partial(\Delta H)}{\partial t} \quad (1)$$

where x, y, z are the Cartesian coordinates, ρ is the density of the material, C_p is the specific heat, k is the heat conductivity, T is the temperature, $\Delta H = f_L L$, L is the latent heat of fusion, and f_L is assumed to vary linearly with temperature in the mushy zone. In the present study, L is 389 kJ/kg.

The heat flux distribution into the keyhole during EBW is a poorly defined function of the coordinates, time and material properties, due to complex interactions occurring in the cavity between the high-energy density electron beam and metal in liquid or vapor state at different temperatures. To simplify the problem and to establish a heat transfer model, the following conditions were assumed: (1) heat flux is a Gaussian distribution centred on the electron beam at any transverse cross-section; (2) reflection from the molten metal surface and the absorption, scattering and radiation within the plasma in the cavity were considered as a uniform distributed heat source.

Accordingly, the heat generated by electron beam consisted of the following two parts: (1) heat generated by bombardment of accelerated electrons onto the surface of the keyhole; (2) heat transferred by vapor and plasma generated by energy input at the bottom of the keyhole.

The first part of the heat can be calculated based on the Gaussian power distribution in the electron beam, which was input in z-axis and moved along x-axis, and can be expressed as

$$q_1(x, y) = \frac{3\eta P}{\pi a^2}\exp\left(-\frac{3r^2}{a^2}\right) \quad (2)$$

where η is the electron beam energy-absorption efficiency of the molten material, and $\eta = 0.7$ in the present work, P is the welding power, a is the radius of the electron beam, this is the distance where the heat input has decreased to 5% and therefore no heat is applied outside this distance in the model, $r = \sqrt{(x - vt)^2 + y^2}$ is the distance from the centre of the electron beam and v is the welding speed.

Considering that the cavity surface is not vertical to the electron input direction, the angle factor must be taken into account. Thus, the Eq. (2) can be rewritten as

$$q_1(x, y) = \frac{3\eta P \sin\theta(x, y, z)}{\pi a^2}\exp\left(-\frac{3r^2}{a^2}\right) \quad (3)$$

where $\theta(x, y, z)$ is the angle between molten metal surface and electron input direction. In Eq. (3), the angle θ is related to the shape of the keyhole, and is programmed by the subroutine of MARC software written in Digital Visual Fortran. As the dimension of the ellipsoidal keyhole was assumed prior to simulation, θ could be written as a function of its position and the size of the keyhole. Fig. 3 shows θ at one point in the cavity.

The second part of the heat was assumed to be a uniformly distributed source, and it was expressed as

$$q_2 = \frac{(1 - \eta)P}{\int ds} \quad (4)$$

where η is the electron beam energy-absorption efficiency of the molten material, P is the welding power and ds is the differential area of the keyhole surface.

Then the total heat flux acting on the workpiece would be written as

$$Q = q_1 + q_2 \quad (5)$$

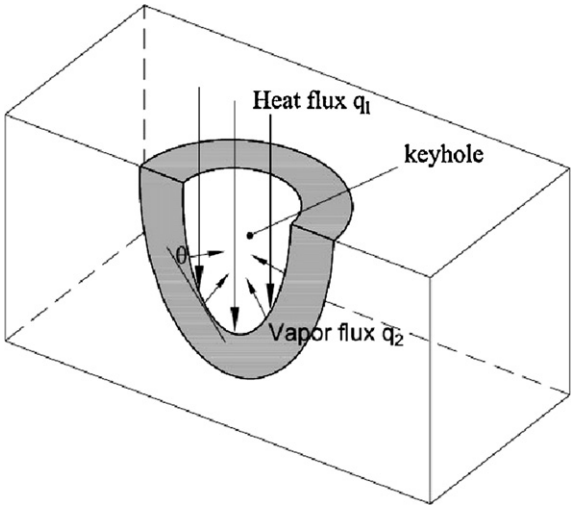

Fig. 3 – Schematic drawing of a keyhole and θ angle between incident beam and cavity surface. The heat flux q_1 indicate the heat generated by bombardment of accelerated electrons, and vapor flux q_2 indicate the heat transferred by vapor and plasma generated by energy input at the bottom of the keyhole.

During the welding process, the heat supplied by the electron beam is conducted to the edges of the workpiece. Radiation losses will occur when there are significant temperature differences between workpiece and environment. Radiation is a principal heat dissipation pathway during vacuum EBW and the boundary condition of heat radiation on the surfaces of the aluminum alloy was defined as

$$q = \varepsilon\lambda(T_s^4 - T_\infty^4) \quad (6)$$

where ε is the heat emissivity, λ is the Stefan–Boltzman constant, T_s and T_∞ are surface and ambient temperature, respectively.

In this simulation, the heat flux q_1 was applied to the total keyhole surface, and q_2 was applied to the bottom of the keyhole, as shown in Fig. 3. The heat flux boundary conditions q_1 and q_2, velocity and path of heat source, and radiation boundary condition q were controlled by subroutines of MARC software written in Digital Visual Fortran.

2.4. *Mechanical analysis*

Mechanical boundary conditions of the finite element model included:

(1) Symmetry displacement boundary condition.
(2) Pre-deformation boundary condition.

During welding, welded structure was confined by clamping fixtures at specific locations which imposed planned displacements in the z-direction. Thus, a pre-deformation was achieved, and the pre-deformation was in a reverse direction to the expected distortion of the welded structure after welding, aiming at decreasing final distortion of welded structure. Pre-deformation was simulated by application of fixed Z displacement boundary conditions at different clamping positions. Fig. 4 shows the pre-deformation boundary conditions of the finite element model added by fixtures at different positions, in which z1, z2, z3, z4 and z5 were 0, −0.5, −1.5, −1 and −2, respectively.

Assuming the original geometry to be symmetric, the finite elements used account only for symmetric deformation, and the deformation of the structure was calculated in a thermo-mechanical coupled method based on the simulating result of temperature field. The constitutive equation applying incremental plasticity theory to the thermal elasto-plastic material

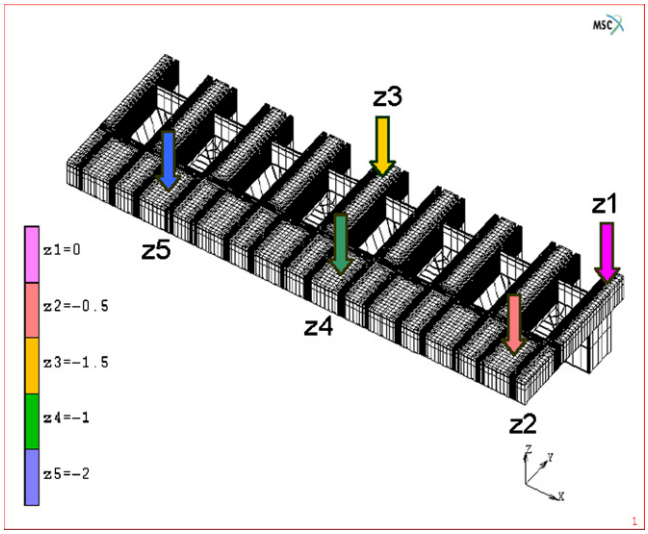

Fig. 4 – Pre-deformation boundary conditions of the finite element model added by the fixture at different positions by imposing different prior displacements in z-direction.

is written as (Chang and Na, 2003):

$$\varepsilon_{ij} = \varepsilon_{ij}^{e} + \varepsilon_{\varepsilon ij}^{P} + \varepsilon_{ij}^{th} \quad (7)$$

where ε_{ij}, ε_{ij}^{e}, $\varepsilon_{\varepsilon ij}^{P}$ and ε_{ij}^{th} are the total, elastic, plastic and thermal strains, respectively.

The transient temperature-dependent and nonlinear structural behavior in welding is computationally represented in the form of nodal displacements during the incremental loading of the finite element model. The incremental plasticity formulation for temperature-dependent equations of thermal elasto-plasticity can be found in the MARC MSC User's Guide Theory and User Information (MARC, 2005).

2.5. *Material properties*

Considering that the temperature gradient is quite large around the welding zone and the material properties change considerably, temperature-dependent thermal properties were used to increase the accuracy of the heat transfer solution. The mechanical properties of the Al alloy were measured experimentally, and were also temperature-dependent. The material properties were not considered as the rate-dependent model in this study. Thermal and mechanical properties of the Al alloy are listed in Table 1.

Table 1 – Thermal and mechanical properties of Al alloy

T (K)	λ (W/m K)	α (×10^{-6} K)	C (J/kg K)	E (GPa)	$\sigma_{0.2}$ (MPa)	ρ (g/cm^3)	υ
298	180.0			47	120	2.74	0.33
373	188.4	23.2	1089	40.8	107		
473	180.0	24.3	1172	40	80		
573	184.2	25.0	1298	40.2	50		
673			1298	38.6	25.7		
773				32.5	17.3		

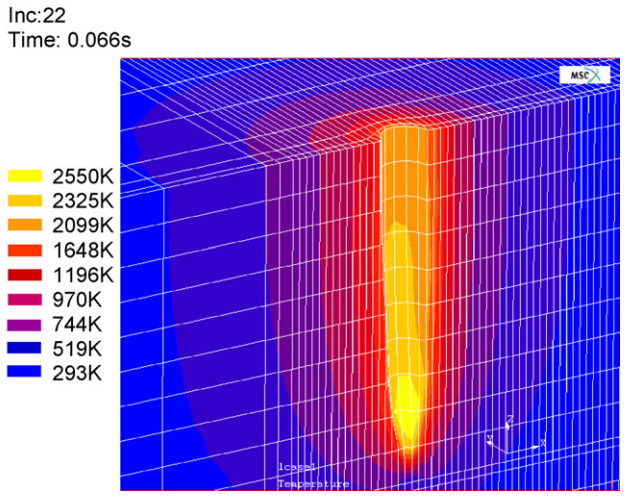

Fig. 5 – Temperature distribution at surface of keyhole.

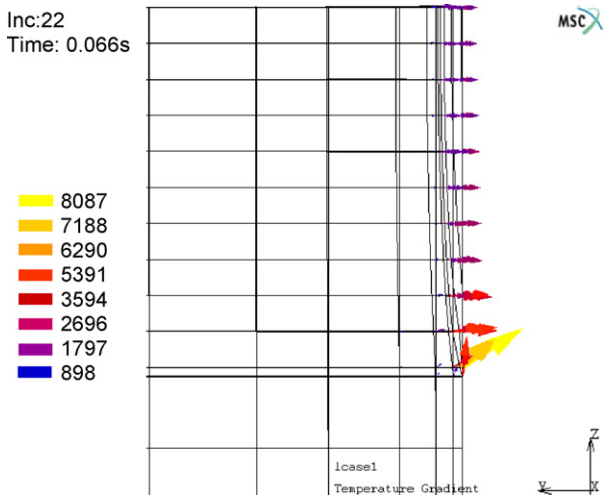

Fig. 6 – Temperature gradient in the cross-section vertical to the welding direction.

3. Results and discussion

3.1. *Results of temperature distribution*

Due to the complex interactions that occur in the keyhole, which mostly depend on the temperature distribution and have a direct effect on the depth of the cavity, it was of great interest to explore the cavity surface temperature. Fig. 5 shows the predicted result of surface temperature distribution of the keyhole, with the parameters of 24 mA welding current, 20 mm/s welding speed and a 4 mm deep keyhole. It can be seen that the highest temperature point, which is up to 2550 K, was modeled to be at the bottom of the cavity's front wall because of the direct bombardment. This may be compared to 2173 K measured during electron beam welding of Al alloy in a previous study (Schauer et al., 1978), therefore the simulation based on the above assumed keyhole and heat source was considered to be a reasonable result. The existence of the keyhole allows the electron beam to put the energy deep into the workpiece body, resulting in a 4.48 mm deep weld pool with only 2.04 mm width according to the isotherm of melting temperature. Fig. 6 depicts the temperature gradient in the cross-section vertical to welding direction. It was found that the direction of the gradient was vertical to the weld pool profile and the numerical value of the gradient increased gradually from the top of the fusion line to the bottom of the weld pool. Fig. 7 gives a comparison of weld pool profile between simulation and experiment. The right side of Fig. 7 is an optical micrograph of the electron beam welded structure by using the same welding current 24 mA and welding speed 20 mm/s, and then the sample was cross-sectioned. The left side of this figure is temperature distribution in the cross-section vertical to the welding direction. Compared with the top surface of the model, the relatively higher heat dissipation in the centre of the workpiece body caused the temperature contour in the weld area to follow a "V" shape, which is in good agreement with the weld pool profile of a sample welded by the same parameters. A good agreement between the measured and calculated weld pool profile indicated that the developed model for the prediction of temperature history provided satisfactory results.

Fig. 8 shows a comparison of temperature–time history of different nodes at different y positions. The curves illustrate that the temperature of the node near the keyhole changed remarkably, especially in the heating process. A much lower temperature rate was achieved when the node was 1.5 mm and 2.3 mm away from the weld centerline. Fig. 9 shows the temperature–time history of nodes along the weld centerline at different z positions. It can be observed that although lower heat flux was input in the region near the top surface of the plate, its temperature was the first to increase. However, the temperature was soon surpassed by that of the nodes near the bottom of the keyhole. Little change occurred at the node 4.5 mm below the weld pool.

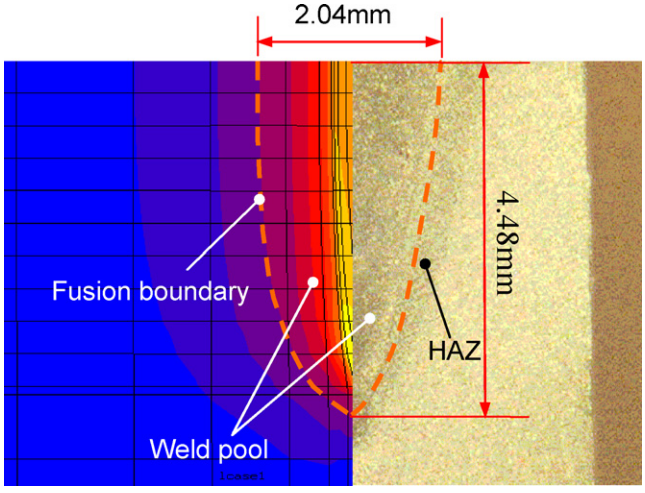

Fig. 7 – Comparison of weld pool profile between simulation and experiment.

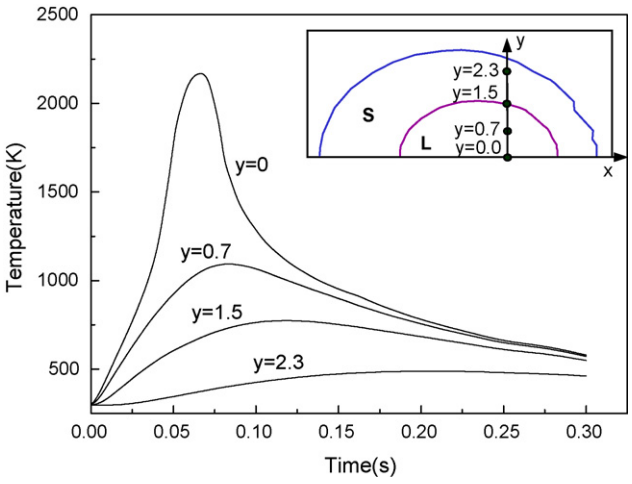

Fig. 8 – Temperature–time history plot of nodes at different y positions.

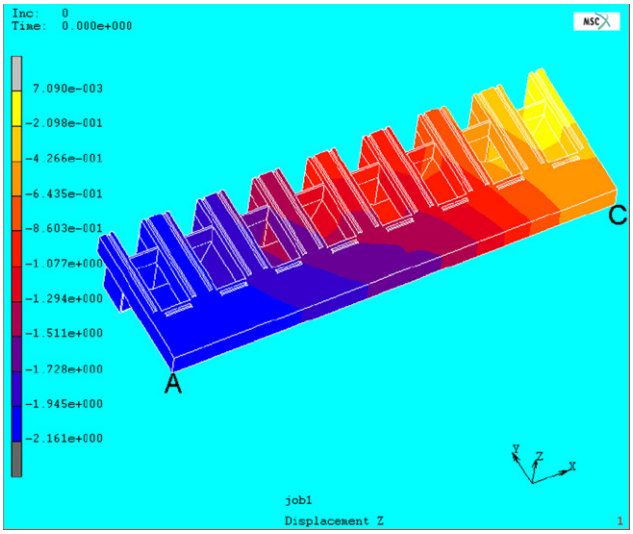

Fig. 10 – Distortion of the Al alloy structure before welding caused by fixture.

3.2. *Distortion of the welded structure*

To demonstrate effects of welding parameters including welding current, welding speed and pre-deformation on distortion of the welded structure, a series of calculations was performed. Fig. 10 shows the z-direction displacement imposed by the fixture before welding, indicates a downward distortion however, when the fixture was removed, the whole structure was distorted upwards.

The data of displacement in the z-direction were extracted along line AC, shown in Fig. 10. Fig. 11 shows the relationship between welding parameters and displacement in z-direction at point A. Fig. 11a shows the effects of welding current on distortion. It was found that the welding current had strong influence on distortion. With the increase of welding current up to 26.4 mA, the distortion of the welded structure increased. Fig. 11b shows the distortion of welded structure at different welding speeds. It was found that the effects of welding speed were not as strong as the effects of welding current. When the heat input was equal, the temperature gradient caused by higher current was larger than that resulting from lower speed, because former provided less time for heat dissipation. As shown in Fig. 11b, with the increase of welding speed up to 25 mm/s, the distortion decreased. It is obvious that higher welding speed decreases the line energy input and results in lower temperature gradients, and hence decreases distortion. Fig. 11c shows the effects of pre-deformation preload on the distortion of welded structure. The range of the prior displacement in z-direction given by the fixture is ±20%. The simulation result show that the final distortion decreased with the increase of the pre-deformation.

Fig. 12 shows the relationship between prior displacement in z-direction added by the fixture and resulting distortion. It was found that larger pre-deformation (indicated by z-direction displacement) resulted in a reduced final distortion.

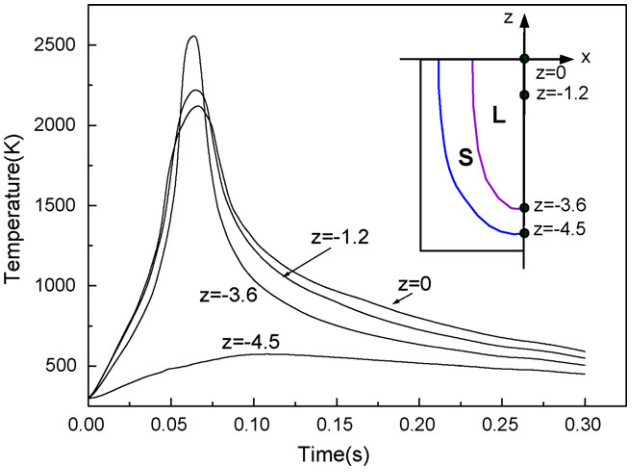

Fig. 9 – Temperature–time history plot of nodes at different z positions.

4. Summary

A computer cluster system including four computers for parallel calculation was established for the finite element modeling of a large and complex Al alloy structure to improve simulation capability and efficiency.

A three-dimensional finite element model included a moving ellipsoidal keyhole developed for EBW of Al alloy. A complex heat source composed of a modified Gaussian distribution heat flux and a uniform heat flux was adopted in this analysis. Results of temperature field simulation showed that the special heat source based on the keyhole caused the weld pool to follow a "V" shape, and the maximum temperature and temperature gradient were at the bottom of the cavity.

Effects of electron beam welding parameters including welding current, welding speed and pre-deformation on final distortion of the welded structure were investigated systematically. The results have shown that heat input was the main factor affecting the magnitude of distortion of the welded structure. With the increase of heat input, the distortion of welded structure increased. The contribution of welding cur-

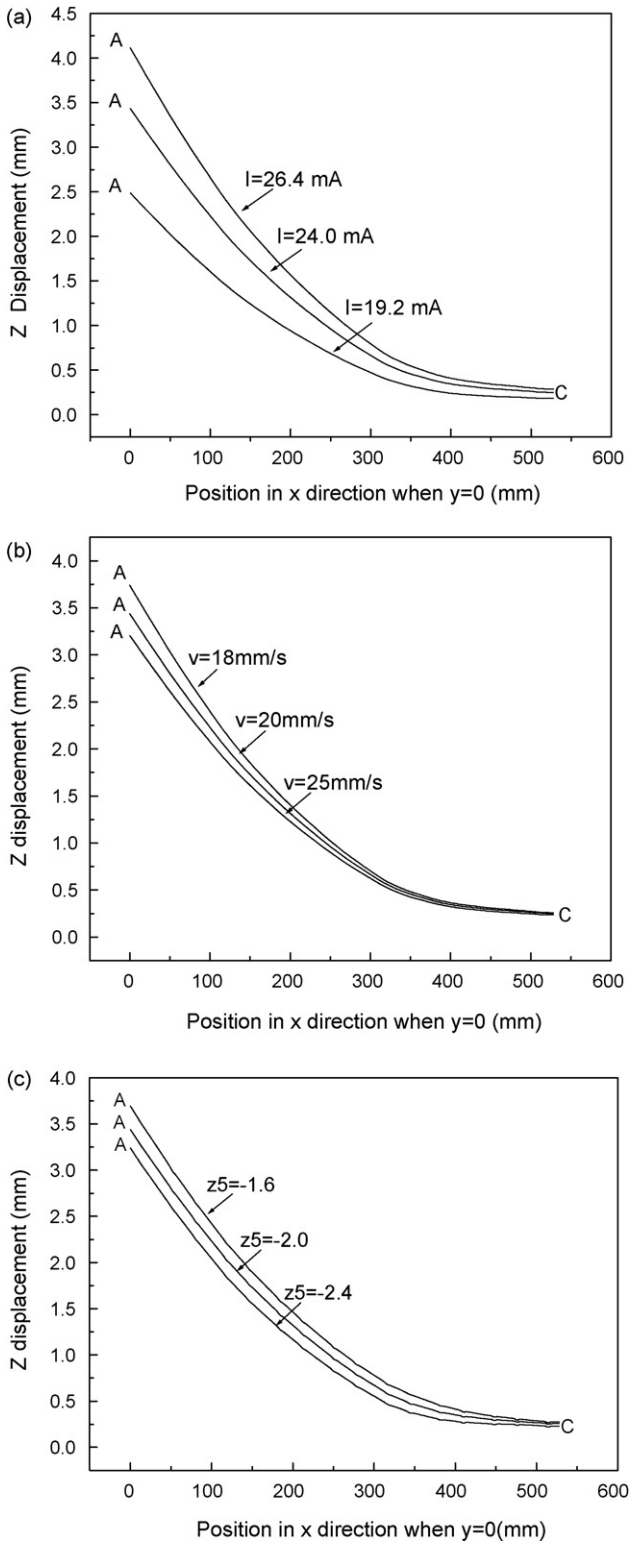

Fig. 11 – Distortion curves along AC after welding when fixture was removed: (a) effect of welding current, (b) effect of welding speed and (c) effect of pre-deformation.

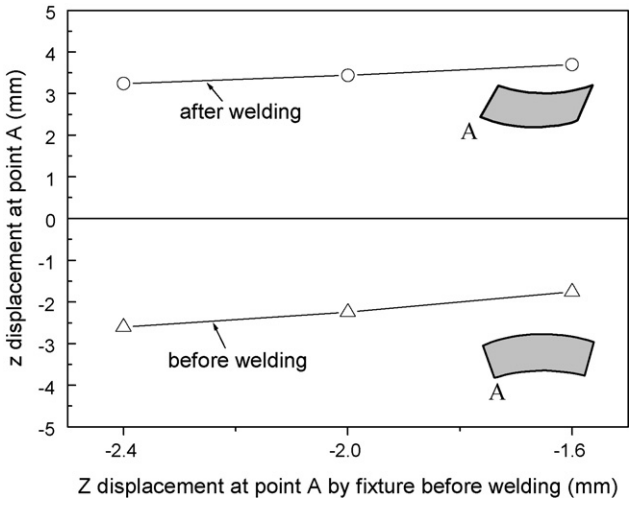

Fig. 12 – Effect of Z displacement added by fixture before welding on pre-deformation and distortion of welding structure.

rent to the distortion was larger than the welding speed. Distortion of the welded structure could be decreased by application of pre-deformation before welding. The distortion after welding decreased with increase of pre-deformation preload before welding.

Acknowledgments

The authors are grateful to Professor W.H. Scott Lawson of University of Waterloo in reviewing the manuscript. The appreciation is also extended to Dr. Xiaogang Li for his valuable comments.

REFERENCES

Baeva, M., Baev, P., Kaplan, A., 1997. An analysis of the heat transfer from a moving elliptical cylinder. J. Phys. D: Appl. Phys. 30, 1190–1196.

Brown, S.B., Song, H., 1992a. Implications of three-dimensional numerical simulations of welding of large structures. Weld. J. 71, 55s–62s.

Brown, S., Song, H., 1992b. Finite element simulation of welding of large structures. J. Eng. Ind. 114, 441–451.

Chang, W.S., Na, S.J., 2003. Thermomechanical analyses of laser precision joining for optoelectronic components. IEEE Trans. Compon. Packag. Technol. 26, 349–358.

Couedel, D., Rogeon, P., Lemasson, P., Carin, M., Parpillon, J.C., Berthet, R., 2003. 2-D-Heat transfer modeling within limited regions using moving sources: application to electron beam welding. Int. J. Heat Mass Trans. 46, 4553–4559.

He, X., DebRoy, T., 2003. Probing temperature during laser spot welding from vapor composition and modeling. J. Appl. Phys. 94, 6949–6958.

Ho, C.Y., Wei, P.S., 1997. Energy absorption in a conical cavity truncated by spherical cap subject to a focused high-intensity beam. Int. J. Heat Mass Trans. 40, 1895–1901.

Lindgren, L.-E., 2001. Finite element modeling and simulation of welding. Part 1. Increased complexity. J. Therm. Stresses 24, 141–192.

Lindgren, L.E., Haggblad, H.A., Mcdill, J.M.J., Oddy, A.S., 1997. Automatic remeshing for three-dimensional finite element simulation of welding. Comput. Methods Appl. Mech. Eng. 147, 401–409.

Lundbäck, A., 2003. Finite Element Modeling and Simulation of Welding of Aerospace Components. Department of Applied Physics and Mechanical Engineering, Luleå University of Technology, Luleå.

MARC, MSC User's Guide. Volume A: Theory and User Information Version 2005.

Miyazaki, T., Giedt, W.H., 1982. Heat transfer from an elliptical cylinder moving through an infinite plate applied to electron beam welding. Heat Mass Trans. 25, 807–814.

Nguyen, N.T., Ohta, A., Matsuoka, K., Suzuki, N., Maeda, Y., 1999. Analytical solutions for transient temperature of semi-infinite body subjected to 3-D moving heat sources. Weld. J., 265s–274s.

Qingyu, S., Anli, L., Haiyan, Z., Aiping, W., 2002. Development and application of the adaptive mesh technique in the three-dimensional numerical simulation of the welding process. J. Mater. Process. Technol. 121, 167–172.

Schauer, D.A., Giedt, W.H., Shintaku, S.M., 1978. Electron beam welding cavity temperature distributions in pure metals and alloys. Weld. J. 57, 127s–133s.

Tong, H., Gied, W.H., 1970. A dynamic interpretation of electron beam welding. Weld. J. 49, 259s–266s.

Wei, P.S., Shian, M.D., 1993. Three-dimensional analytical temperature field around the welding cavity produced by a moving distributed high-intensity beam. J. Heat Trans. 115, 848–855.